Journal of Biomedical Optics

SPIEDigitalLibrary.org/jbo

Collagen I fiber density increases in lymph node positive breast cancers: pilot study

Samata M. Kakkad
Meiyappan Solaiyappan
Pedram Argani
Saraswati Sukumar
Lisa K. Jacobs
Dieter Leibfritz
Zaver M. Bhujwalla
Kristine Glunde

SPIE

Collagen I fiber density increases in lymph node positive breast cancers: pilot study

Samata M. Kakkad,[a,e] Meiyappan Solaiyappan,[a] Pedram Argani,[b,d] Saraswati Sukumar,[b,d] Lisa K. Jacobs,[b,c] Dieter Leibfritz,[e] Zaver M. Bhujwalla,[a,b] and Kristine Glunde[a,b]

[a]The Johns Hopkins University School of Medicine, In Vivo Cellular and Molecular Imaging Center, Division of Cancer Imaging Research, The Russell H. Morgan Department of Radiology and Radiological Science, Baltimore, Maryland
[b]The Johns Hopkins University School of Medicine, The Sidney Kimmel Comprehensive Cancer Center, Baltimore, Maryland
[c]The Johns Hopkins University School of Medicine, Department of Surgery, Baltimore, Maryland
[d]The Johns Hopkins University School of Medicine, Pathology Department, Baltimore, Maryland
[e]University of Bremen, Department of Chemistry and Biology, Bremen, Germany

Abstract. Collagen I (Col1) fibers are a major structural component in the extracellular matrix of human breast cancers. In a preliminary pilot study, we explored the link between Col1 fiber density in primary human breast cancers and the occurrence of lymph node metastasis. Col1 fibers were detected by second harmonic generation (SHG) microscopy in primary human breast cancers from patients presenting with lymph node metastasis (LN^+) versus those without lymph node metastasis (LN^-). Col1 fiber density, which was quantified using our in-house SHG image analysis software, was significantly higher in the primary human breast cancers of LN^+ (fiber volume = 29.22% ± 4.72%, inter-fiber distance = 2.25 ± 0.45 μm) versus LN^- (fiber volume = 20.33%± 5.56%, inter-fiber distance = 2.88 ± 1.07 μm) patients. Texture analysis by evaluating the co-occurrence matrix and the Fourier transform of the Col1 fibers proved to be significantly different for the parameters of co-relation and energy, as well as aspect ratio and eccentricity, for LN^+ versus LN^- cases. We also demonstrated that tissue fixation and paraffin embedding had negligible effect on SHG Col1 fiber detection and quantification. High Col1 fiber density in primary breast tumors is associated with breast cancer metastasis and may serve as an imaging biomarker of metastasis. [DOI: 10.1117/1.JBO.17.11.116017]

Keywords: Collagen I; fiber; breast cancer; lymph node metastasis; second harmonic generation microscopy.

Paper 11731 received Dec. 8, 2011; revised manuscript received Sep. 16, 2012; accepted for publication Oct. 5, 2012; published online Nov. 1, 2012.

1 Introduction

The extracellular matrix (ECM) in primary breast cancers is significantly altered compared with normal breast tissue and may provide new biomarkers for cancer diagnosis,[1–4] metastasis prediction,[5,6] and prognosis of survival.[7] Cancer metastasis is a multistep process in which the tumor microenvironment (TME) facilitates cancer cell–ECM interactions that are necessary for metastasis to occur.[8] The ECM in breast tumors is composed of a complex meshwork of fibrillar collagens, glycoproteins, and proteoglycans,[9] which profoundly affect metastasis, as well as proliferation, angiogenesis, adhesion, migration, invasion, macromolecular transport, and drug delivery.[9–13] Multiple molecular mechanisms, such as ECM degradation by proteases secreted by cancer cells and dysregulated ECM synthesis by tumor-associated stromal cells, have been implicated in the formation of the significantly altered ECM of breast tumors[8] that include structural changes in the fiber patterns of fiber-forming ECM components. Collagen I (Col1) fibers are the major structural ECM component in breast tumors,[5,6,9,14,15] and increased stromal Col1 has been found to facilitate breast tumor formation, invasion, and metastasis.[5,6]

Address all correspondence to: Kristine Glunde, The Johns Hopkins University School of Medicine, Department of Radiology, 212 Traylor Building, 720 Rutland Avenue, Baltimore, Maryland 21205. Tel: (410) 614-2705; Fax: (410) 614-1948; E-mail: kglunde@mri.jhu.edu, or Zaver M. Bhujwalla, The Johns Hopkins University School of Medicine, Department of Radiology, 208C Traylor Building, 720 Rutland Avenue, Baltimore, Maryland 21205. Tel: (410) 955-9698; Fax: (410) 614-1948; E-mail: zaver@mri.jhu.edu.

X-ray mammography, which detects radiodense fibroglandular tissue in the breast, demonstrated that women with high (50% to 74% versus <5%) breast density have a 4.64-fold increased risk of developing breast carcinoma.[16,17] Histologic evaluation of biopsy and mastectomy specimens from x-ray mammographically dense breast regions revealed a significantly higher collagen density and extent of fibrosis in these regions.[14,15] High Col1 fiber density significantly increased mammary tumor initiation, progression, and lung metastasis.[6] Cancer cell invasion in this mouse model started at the tumor–stromal interface in the primary tumor along radially aligned Col1 fibers, which can form avenues for metastasis.[5] In a recent study, Col1 fibers that were oriented perpendicular to the cancer cell boundaries were found to serve as a prognostic signature for survival of breast carcinoma patients.[7]

Here we have, for the first time, performed a pilot study to test the relationship between lymph node metastasis and Col1 fiber texture and density in primary human breast cancers using second harmonic generation (SHG) microscopy. SHG microscopy detects an intrinsic signal generated by the noncentrosymmetric physical properties of Col1 fibers and does not require the use of an exogenous optical imaging agent.[3,4,18] We have performed a small retrospective SHG microscopy study to determine if the Col1 fiber signature in primary breast tumors is altered in patients presenting with lymph node metastasis (LN^+) compared to patients with uninvolved lymph nodes

0091-3286/2012/$25.00 © 2012 SPIE

(LN^-). We used our in-house automated fiber analysis software as previously described,[19] which is free of user variability, and observed that primary breast cancers in LN^+ patients have significantly denser Col1 fiber signatures than primary breast cancer in LN^- patients. To validate our in-house software results, we additionally used two commonly used texture analysis techniques to analyze Col1 images:[20–22] the gray level co-occurrence matrix (GLCM) and the Fourier transform (FT). We observed that the GLCM parameters, co-relation and energy, and the FT parameters, aspect ratio and eccentricity, were significantly different for the Col1 fiber distribution in LN^+ cases compared to the LN^- cases. We also demonstrated that tissue fixation and paraffin embedding had no effect on SHG Col1 fiber detection and quantification, indicating that Col1 fiber assessment by nondestructive SHG microscopy may be implemented in routine clinical pathology settings.

2 Materials and Methods

2.1 *Ethics Statement*

An exemption for retrospective analysis of de-identified human breast tumor specimens was approved by the Institutional Review Board of the Johns Hopkins University School of Medicine as these specimens were not collected specifically for this particular research project, and the identity of the individuals to whom the specimens pertain was unknown to everyone involved in this research project. Research that involves only coded human biological specimens is not human subjects research under the human subjects regulations of the US Department of Health and Human Services.

All experimental animal protocols were approved by the Institutional Animal Care and Use Committee of the Johns Hopkins University School of Medicine under the animal protocol number MO08M166 and under the Animal Welfare Assurance Number A3272-01.

2.2 *Tumor Xenograft Specimens*

To test if different types of tissue processing affect the SHG Col1 fiber signals, we used a xenograft model system of human breast tumors instead of valuable patient material. MCF-7, a nonmetastatic, estrogen-sensitive (estrogen-dependent) line, was orthotopically inoculated in the upper left thoracic mammary fat pad of female athymic nude mice to grow breast tumor xenografts. MCF-7 breast cancer cells were purchased from American Type Culture Collection (ATCC) and used within 6 months. The MCF-7 cell line was tested and authenticated by ATCC by two independent methods: the ATCC cytochrome C oxidase I polymerase chain reaction (PCR) assay and short-tandem-repeat profiling using multiplex PCR. For MCF-7 cell inoculations, 0.18 mg of a 60-day release 17 β-estradiol pellet (Innovative Research of America) was subcutaneously implanted near the left shoulder of athymic nude mice 1 week before inoculation. Two million MCF-7 cells were inoculated in a volume of 0.05 mL Hanks balanced salt solution (HBSS) (Sigma; no Matrigel was used). Tumor size was about 500 mm^3 when animals were killed and tumors were removed. To assess if tissue processing affects SHG-detected Col1 fiber patterns, each tumor was cut into three equal-sized parallel pieces. One piece was formalin-fixed paraffin-embedded (FFPE), a second piece was put on a microscope slide and kept in an ice-box for immediate fresh-tissue SHG imaging, and a third piece was placed in Tissue Tek OCT™ freezing compound (Sakura Finetek USA, Torrance, CA), cryosectioned with a microcryotome (Microm International, Walldorf, Germany) at 100-μm thickness, fixed with 4% paraformaldehyde (Sigma-Aldrich) solution, and mounted with Faramount aqueous mounting medium (DakoCytomation, Carpinteria, CA).

2.3 *Breast Cancer Specimens*

We retrospectively analyzed 14 breast cancer tissues, all of which were invasive ductal carcinomas (IDC). Eight of these breast cancers were LN^+ and six were LN^-. All cancers were tumor grade 2 to 3, estrogen receptor positive (ER^+), and progesterone receptor positive (PR^+). All of our samples were obtained from hospitals in Maryland and were graded by board-certified breast pathologists including P. Argani. Snap-frozen primary breast tumor specimens were placed in Tissue Tek OCT freezing compound (Sakura Finetek USA), cryosectioned with a microcryotome (Microm International) at 100-μm thickness for whole-mount sections and 5-μm thickness for adjacent sections, fixed with 4% paraformaldehyde (Sigma-Aldrich) solution, stained for nuclei with Hoechst 33342 (Invitrogen, Carlsbad, CA), and mounted with Faramount aqueous mounting medium (DakoCytomation) as previously described.[19] For testing the within-tumor consistency of SHG-detected Col1 inter-fiber distances and Col1 fiber volume, we obtained FFPE samples from four different biopsy passes of the same breast cancer for four human specimens, which were grade 3, LN^+, ER^+, and PR^+; grade 2, LN^+, ER^+, PR^+; grade 2, LN^-, ER^+, PR^+; and grade 3, LN^+, ER^+, PR^-. These FFPE samples were embedded in paraffin blocks, within which they were marked with the pink dye phloxine, which visualizes the shape of the biopsy specimen within the white paraffin block. We also obtained the adjacent hematoxylin and eosin (H&E) slide. In our pathology lab, the H&E section is always cut as the last slide in the series from a given FFPE block. Therefore it was possible to spatially correlate the shape of the H&E section with the specimen in the FFPE block.

2.4 *SHG Imaging*

SHG microscopy was performed on a Zeiss LSM 710 NLO Meta confocal microscope (Carl Zeiss MicroImaging, Thornwood, NY) equipped with a 680- to 1080-nm tunable Coherent Chameleon Vision II laser with automated pre-compensation (Coherent, Santa Clara, CA) located in the Johns Hopkins University School of Medicine (JHU SOM) Microscope Core Facility (directed by Dr. Scot Kuo). Incident laser light of 880 nm was used for generating the SHG Col1 signal and laser light of 760 nm for two-photon excitation of Hoechst 33342. The laser power used was about 10 mW for the 880-nm channel and about 19 mW for the 760-nm channel. The SHG signal was detected within 410 to 450 nm, and the Hoechst fluorescence was detected within 400 to 475 nm. Six to 10 random fields of view (FOVs) per sample that were equidistantly spread throughout the breast tumor specimen were imaged to provide a realistic representation of each breast cancer sample. At each FOV, we acquired a z-stack of 100 μm total thickness with a z-interval of 5 μm using a $25\times/0.8$ LD LCI PlanApo multi-immersion lens. The corresponding images of adjacently cut, H&E-stained, 5-mm-thick sections were used to verify that all samples contained cancer. Brightfield microscopy of the H&E-stained adjacent sections was performed using a Nikon

inverted microscope equipped with a Nikon Coolpix digital camera (Nikon Instruments, Melville, NY). For testing the within-tumor consistency using FFPE blocks of different biopsy passes, we additionally performed tile-function imaging covering the entire biopsy sample for two biopsy passes, again acquiring z-stacks of 100 μm total thickness with a z-interval of 5 μm using the 25× lens.

2.5 *Col1 Fiber Quantification*

To quantify our data independent of SHG signal intensity and free of errors introduced by user variability, we used automated geometric analysis and texture analysis techniques. We used a geometric analysis technique in which the parameters of fiber volume and inter-fiber distance were calculated. Image analysis to quantify the Col1 inter-fiber distance and the Col1 fiber volume was performed using in-house software as previously described.[19] This software was written in Matlab (version 7.4.0, TheMathWorks, Natick, MA) and was previously described in detail.[19] Briefly, our software quantifies the median of all Col1 inter-fiber distances and the total Col1 fiber volume as outlined in Fig. 1. A representative z-plane of a raw image is shown in Fig. 1(a), which is preprocessed to exclude noise and nonfibrillar shapes as demonstrated in the schematic in Fig. 1(b), resulting in the extraction of Col1 fiber structures from the raw images as shown in Fig. 1(c). As indicated in Fig. 1(d), Euclidean distances from each empty voxel to the nearest Col1 fiber voxel were computed within each 3-D FOV to quantify the inter-fiber distances and the total fiber volume from the Col1 fiber mesh. Based on a previous report, we expected more tightly packed Col1 fibers and a higher fiber volume for LN^+ cases as compared to LN^- cases.[6] Therefore, a one-sided t-test ($\alpha = 0.05$) was used to detect significant differences in the Col1 inter-fiber distance and the Col1 fiber volume between primary tumors from LN^- versus LN^+ cases using Excel 2007 (Microsoft, Redmond, WA). P values of <0.05 were considered to be significant. P values of $0.10 > P > 0.05$ were considered to be a trend toward significance.[23]

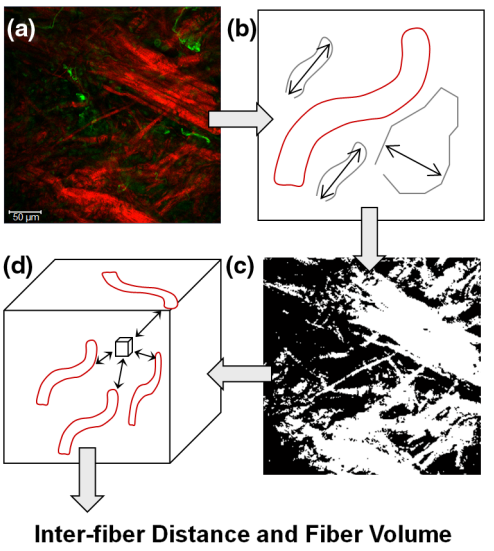

Fig. 1 Construction of inter-fiber distance and fiber volume. Composite image (a) of the collagen I (Col1) fibers (red) and cell nuclei (green); preprocessing using the optional filter (b) to identify fiber-like objects (red) among various non-fiber-like objects in the image to produce the corresponding Col1 fiber image (c); (d) computing the distances from each 3-D voxel to the surrounding fibers in 3-D to determine the nearest distance to a fiber in μm and the total fiber volume (%). One z-plane from a 3-D image stack is displayed in (a) and (c). Each image size is 339 by 339 μm. The scale bars represent 50 μm.

To validate our analysis results, we also used well-established texture analysis methods for Col1 fiber quantification,[20–22] to see whether the Col1 fiber distributions were significantly different for the LN^- and LN^+ cases as observed in our geometric analysis. We used GLCM and FT texture analysis to analyze Col1 fiber distributions. Several textural features were extracted by GLCM, which is a statistical texture analysis method based on the second-order statistics of an image's gray-scale histogram.[24] This analysis was done in Matlab. The extracted features include (1) contrast, which is a measure of intensity variation, with a contrast = 0 for a constant image, and a range = [0 1]; (2) co-relation, which is a measure of how a pixel is co-related to its neighboring pixel, with 1 for positively and −1 for negatively co-related pixels, and a range = [−1 1]; (3) energy, which is also known as uniformity or angular second moment, with an energy = 1 for a constant image, and a range = [0 1]; and (4) homogeneity, which is a property measure of how homogeneous an image is, with a value = 1 for a constant image, and a range = [0 1].[25] We also calculated the 2-D FT for all images. For randomly distributed Col1 fibers, the resulting FT approximates a circle, whereas for a more organized fiber pattern, the FT looks elliptical. FT features were obtained by fitting an ellipse to the FT of each image and including (1) aspect ratio (AR), which is the ratio of the major axis to the minor axis of the ellipse; (2) orientation, which is the angle between the x-axis and the major axis of the ellipse; and (3) eccentricity, which is the ratio of the distance between the foci of the ellipse and the length of the major axis. For a circle, the eccentricity is 0 and its range = [0 1]. A one-sided t-test ($\alpha = 0.05$) was used to detect significant differences in the Col1 texture for all above parameters between primary tumors from LN^- versus LN^+ cases using Excel 2007. P values of < 0.05 were considered to be significant.

3 Results

To test whether the SHG microscopic detection of Col1 fiber signatures depends on tissue processing, we compared fresh tissue samples with formaldehyde-fixed, Hoechst-stained whole-mount sections and FFPE samples from the same MCF-7 breast tumor xenograft. The data presented in Fig. 2 demonstrate that SHG microscopy effectively revealed Col1 fiber signatures in this breast tumor xenograft model. We found that the Col1 fiber distribution in tissues under these different preparations were fairly consistent. Figure 2(a) to 2(c) shows that the Col1 fiber structures were stable and remained unaltered in the same MCF-7 breast tumor xenograft that was first imaged fresh, and from which adjacent sections were re-imaged after 4% paraformaldehyde fixation and Hoechst 33342 staining, or after formalin fixation and paraffin embedding within FFPE blocks. The Col1 fiber volume [Fig. 2(d)] and inter-fiber distance [Fig. 2(e)] from five randomly selected FOVs detected from each sample preparation revealed no changes between the same tissue that was fresh, fixed, or paraffin-embedded. These results suggest that tissues with different preparations (fresh, fixed, or FFPE) can be used for SHG-Col1 imaging studies without introducing artifacts, although in practice, tissue processing within each experimental setup should be kept consistent to avoid any potential variations across different types of tissue preparations.

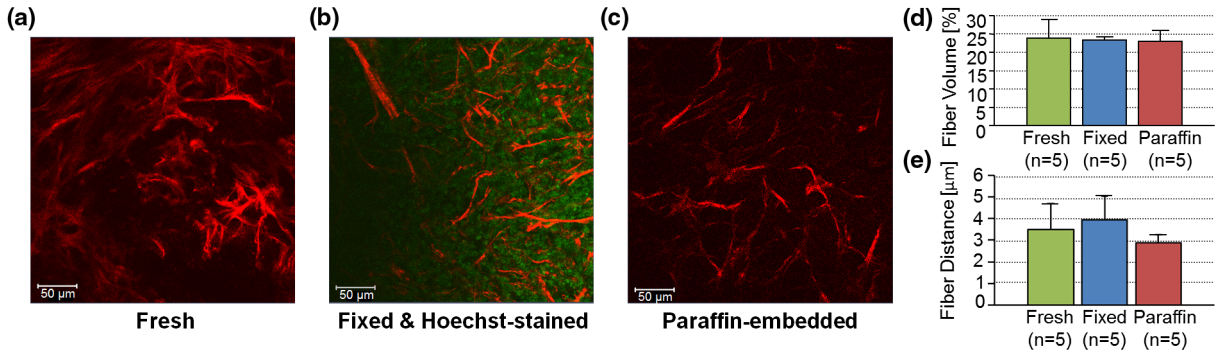

Fig. 2 The second harmonic generation (SHG) signal is robust and independent of tissue processing. We obtained comparable images from fresh (a), fixed and Hoechst-stained (b), and paraffin-embedded (c) MCF-7 breast tumor xenograft tissue, consistent with almost identical results obtained by fiber volume (d) and inter-fiber distance quantification (e) of five randomly selected fields of view (FOVs) from each differently processed tissue. Each image size is 339 by 339 μm. The scale bars represent 50 μm.

We compared the Col1 fiber signatures in the primary tumors of LN^- and LN^+ patients in an initial proof-of-principle pilot study. As evident in Fig. 3, denser SHG Col1 fiber signatures were detected in primary tumor specimens from eight LN^+ patients compared to those from six LN^- patients. We quantified 10 randomly selected, equidistant FOVs from each primary tumor to assess global Col1 changes. This approach accounts for the possibility that Col1 fiber architecture can be spatially heterogeneous within a given tumor. The image quantification software described above was used to quantify the Col1 fiber volume [Fig. 3(c)] and distance [Fig. 3(d)] in this geometric analysis. The Col1 fiber volume significantly ($P = 0.0036$, $n = 6$ to 8, values are mean $\pm$ standard deviation) increased from $20.33\% \pm 5.56\%$ in LN^- to $29.22\% \pm 4.72\%$ in LN^+ patients. The Col1 inter-fiber distance showed a trend toward significance ($P = 0.0807$, $n = 6$ to 8) and decreased from 2.88 ± 1.07 μm in LN^- to 2.25 ± 0.45 μm in LN^+ patients (Fig. 3). The primary tumors of all patients were positive for ER and PR. Hence ER and PR status were the same in all patients and were not confounding factors in this comparison.

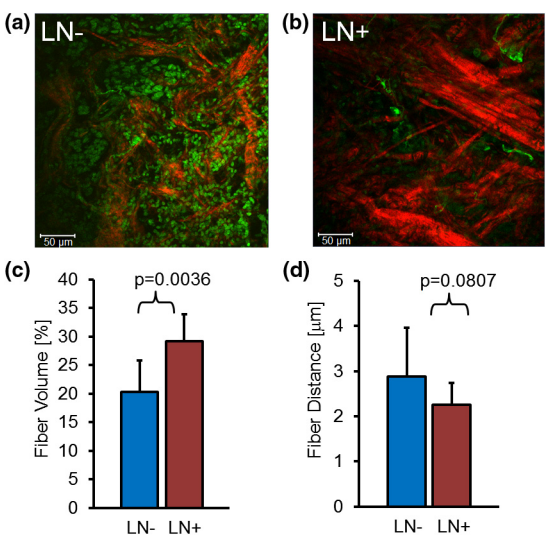

Fig. 3 Primary breast tumors from lymph node positive (LN^+) patients contained denser Col1 fibers than primary tumors from LN^- patients. Shown are representative SHG Col1 fiber (red) images from an LN^- patient (a) and an LN^+ patient (b). Nuclei were counterstained with Hoechst (green). Each image size is 339 by 339 μm; one z-plane is displayed. The scale bars represent 50 μm. LN^- patients ($n = 6$) displayed significantly ($P = 0.0036$) decreased fiber volume (c) and a trend ($P = 0.0807$) toward increased inter-fiber distance (d) compared to LN^+ patients ($n = 8$). Values are mean $\pm$ standard deviation.

To validate our geometric analysis of the differences observed in Col1 fiber distribution of LN^- versus LN^+ patients, we used different texture analysis methods to quantify the fiber patterns in a manner that is independent of the SHG signal intensity. We analyzed the same FOVs as for the geometric analysis using GLCM and FT methods. We observed that the GLCM parameters co-relation and energy [Fig. 4(a)] significantly separated the LN^- and LN^+ patients ($P = 0.0007$ and 0.0178, respectively). The Col1 fibers in LN^- samples had a significantly lower co-relation (LN^- mean = 0.44, LN^+ mean = 0.67, $P = 0.0007$) and a significantly higher energy value (LN^- mean = 0.47, LN^+ mean = 0.28, $P = 0.0178$) than the fibers in LN^+ samples. These parameters of higher co-relation and lower energy in LN^+ versus LN^- cases indicate that LN^+ samples had more and denser Col1 fibers than LN^- samples, which is consistent with our geometric analysis results. In Fig. 4(b), we show that the FT parameters AR and eccentricity were significantly different for the LN^- and LN^+ patient samples ($P = 0.0557$ and 0.0462, respectively). The LN^- samples had a significantly higher AR (LN^- mean = 1.9, LN^+ mean = 1.45, $P = 0.0557$) and a significantly higher eccentricity (LN^- mean = 0.74, LN^+ mean = 0.66, $P = 0.0462$) than the LN^+ samples. The FT analysis parameters AR and eccentricity were able to distinguish between LN^+ and LN^- samples. However, because the spatial information is lost in FT analysis, it was

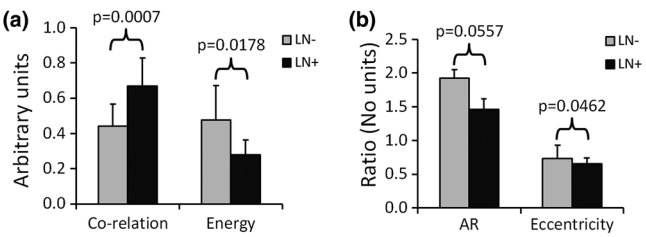

Fig. 4 Gray level co-occurrence matrix (GLCM) and Fourier transform (FT) texture analyses of Col1 fibers in primary breast tumors were able to distinguish between LN^+ and LN^- patients. (a), GLCM parameters showed that LN^- patients ($n = 6$) displayed a significantly decreased inter-fiber co-relation ($P = 0.0007$) and significantly higher energy uniformity ($P = 0.0178$) compared to LN^+ patients ($n = 8$). (b), Texture analysis using FT demonstrated that the Col1 fiber distribution of LN^- patients ($n = 6$) had a significantly higher aspect ratio (AR, $P = 0.0557$) and significantly higher eccentricity value ($P = 0.0462$) compared to LN^+ patients ($n = 8$). Values are mean $\pm$ standard deviation.

not possible in our case to interpret the decrease in AR and eccentricity in LN^+ versus LN^- patients in terms of geometric fiber parameters.

To assess whether local Col1 fiber differences in a given tumor affect global Col1 fiber measurements obtained by analyzing and quantifying 10 randomly selected, equidistant FOVs from each primary tumor ($n = 14$), we determined the spatial heterogeneity of the Col1 fiber architecture in breast tumor specimens. This assessment is necessary because with microscopic techniques such as SHG Col1 fiber imaging, the FOV is in the range of hundreds of microns, whereas clinical breast tumors typically span larger diameters. Therefore, it is necessary to test whether the differences in Col1 fiber density globally span the tumor or are local phenomena. Our data presented in Fig. 5 show that the Col1 inter-fiber distance distribution and fiber volume are almost identical in four biopsy passes that were obtained from the same human breast tumor specimen. In addition, the overall averages of a Col1 fiber volume of $25\% \pm 3\%$ and distance of 3.0 ± 0.4 μm for the tile-imaged biopsy pass B1 are comparable to the averages from six FOVs per biopsy pass (Fig. 5). Comparable results were obtained for a total of four primary breast tumor cases, in which the Col1 fiber volumes and inter-fiber distances for six equidistant FOVs from four separate biopsy passes from each one of the four tumors gave comparable results (null hypothesis of the t-test was true, i.e., $P > 0.05$ for all breast tumor cases; $n = 4$). Although there is some heterogeneity in the Col1 fiber architecture in breast tumor specimens, our approach of measuring and averaging over several randomly selected, equidistant FOVs that cover the entire tumor/biopsy averages out local fiber heterogeneity and detects overall global changes in Col1 fiber signature. Our data indicate that global Col1 fiber alterations in breast tumors dominate local Col1 fiber differences.

4 Discussion

The presence or absence of metastases in axillary lymph nodes is currently the most important predictor of prognosis in breast carcinoma and an integral component of the breast cancer staging system.[26,27] Using *ex vivo* primary tumor specimens from patients, we observed increased Col1 fiber density in LN^+ compared to LN^- patients ($P = 0.0036$, $n = 14$) and significantly varied fiber distributions as obtained by our texture analysis (co-relation, $P = 0.0007$; energy, $P = 0.0178$; AR, $P = 0.0557$; eccentricity, $P = 0.0462$; $n = 14$). Our data are in good agreement with a recent study that identified a tumor-associated Col1 signature (TACS) of bundles of straightened and aligned Col1 fibers that are oriented perpendicular to the tumor boundary as an independent prognostic marker for poor survival in patients with this TACS in their primary tumors.[7] While this larger clinical study scored for disease-free survival in 196 patient samples on human breast carcinoma tissue microarrays, our study more specifically compared primary tumors from LN^+ and LN^- patients in an initial proof-of-principle study. Unlike the study by Conklin et al.[7] that relied on a qualitative yes/no judgment performed by trained persons without software involvement or quantification, data analysis in our study was done by using in-house automated software that quantifies inter-fiber distance and fiber volume from raw Col1-SHG images. A major advantage of this automated analysis approach is that it is free of errors from subjective judgement, and it can give quantitative results in real time. By averaging over 6 to 10 FOVs that were equidistantly spread throughout each breast tumor specimen, we were able to obtain robust quantitative results ($n = 14$, total number of tissue samples). Our data are also in good agreement with preclinical findings in a bi-transgenic mouse model, in which high Col1 fiber density promoted mammary tumor initiation, progression, and metastasis,[6] and provide the first patient data linking lymph node

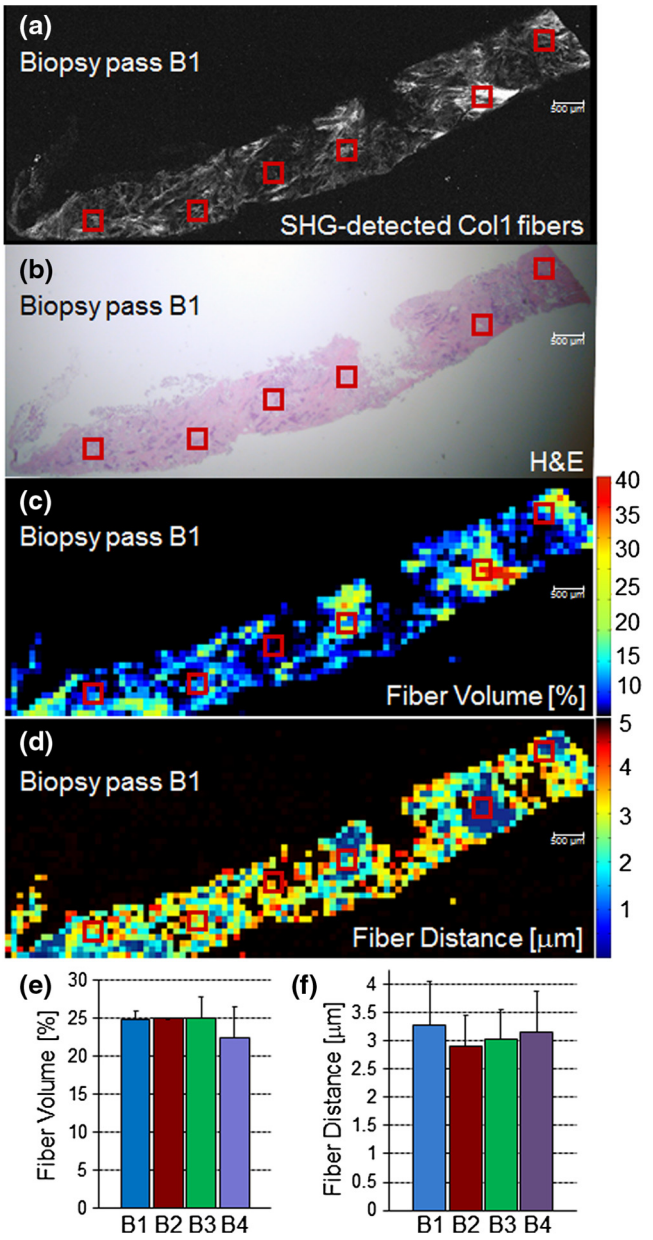

Fig. 5 SHG tile imaging covering breast tumor biopsy B1 (a) and the adjacent hematoxylin and eosin–stained section (b). Fiber volume (c) and fiber distance (d) were quantified with our software on an FOV-by-FOV basis covering the entire biopsy pass B1 to visualize the spatial heterogeneity by heat maps. Representative, average fiber volume and inter-fiber distance of the 3-D data stack is displayed in 2-D [(c) and (d)]. Six randomly selected FOVs (marked in red) in this biopsy were analyzed for their Col1 fiber distribution. Four biopsy passes B1 (shown), B2, B3, and B4 taken from the same LN^+ breast tumor were analyzed for their Col1 fiber volume (e) and distance (f) and displayed close to identical values for both parameters. Values are mean $\pm$ standard deviation. These findings demonstrate that robust global changes in Col1 fiber architecture occur in malignant breast tumors, which can be reliably quantified by randomly selecting six FOVs. Each image size is 9862 by 4080 μm. The scale bars represent 500 μm.

metastasis with Col1 fiber density. In addition, recent studies demonstrated that high Col1 fiber density in primary tumors can facilitate metastasis by providing dense Col1 fiber avenues along which cancer cells migrate to ultimately establish distant colonies.[5,6] In these studies, the initial invasion of breast cancer cells at the tumor–stromal interface was shown to occur along radially aligned Col1 fibers in the primary tumor.[5,6] Breast cancer cells invade into Col1 matrices by overexpressing integrins on their cell surface, which enable these cells to adhere to the Col1-containing ECM.[28,29] Cancer cells migrate through lymphatic vessels to the connected sentinel lymph node to establish metastatic growth.[30–33] Because lymphatic vessels are attached to collagen through anchoring filaments,[34–36] future studies should focus on identifying if Col1 fibers guide migrating cancer cells into tumor-associated lymphatic vessels within the primary tumor.

In the clinic, lymph node status is typically assessed by a sentinel lymph node biopsy, where the sentinel nodes draining the lymphatic basin containing the tumor are identified and excised. This biopsy is typically performed at about 3 weeks after the initial breast biopsy[27] to identify and histologically examine axillary lymph nodes that are at high risk of containing cancer cells. There is a 25% adverse event rate after sentinel lymph node biopsy, with 9% of patients having axillary paresthesia, 6% lymphedema, 6% axillary seromas, and 3% wound infections.[27] Avoiding the sentinel lymph node biopsy procedure would eliminate these risks for those patients that are LN^-. If the sentinel lymph nodes cannot be identified, additional axillary lymph node dissection is performed, which causes even more adverse surgical effects than the sentinel lymph node biopsy alone.[27] Therefore, novel biomarkers that alone or when integrated with other standard markers accurately predict for lymph node metastasis are critically needed. Our data suggest that SHG imaging of Col1 fibers may serve as a surrogate marker to predict the presence of lymph node metastasis, which is in good agreement with the study by Conklin et al.[7] that showed that a specific TACS was able to predict survival. Col1 fibers were detected by optical SHG microscopy, a highly sensitive and nondestructive technique that images intrinsic signal from Col1 fibers.[4,18,37,38] Several other breast cancer markers have been associated with axillary lymph node metastasis such as CCND1, CD44, COX-2, EGFR, HER2/NEU, HPA, and LYVE-1 (reviewed in Ref. 39). In addition, increased expression of vascular endothelial growth factor C (VEGF-C) or VEGF-A, both of which are able to promote lymphangiogenesis in primary tumors, was correlated with an increased incidence of regional lymph node as well as distant metastases in humans and animals.[30–32] Different techniques assessing protein expression, mRNA expression, chromosome alterations, and DNA copy number changes are being used to evaluate these markers of lymph node metastasis in primary breast tumors.[39] The advantage of SHG detection of Col1 fibers as a biomarker of lymph node metastasis is that the technique is nondestructive and can be used to interrogate live tissues.

Our data show that the global Col1 fiber architecture in a given breast cancer is an important parameter that dominates local Col1 fiber differences within the tissue. Our approach of probing several randomly selected, equidistant FOVs covering the entire tumor/biopsy to average out local fiber heterogeneity ensures that we are measuring global Col1 fiber architecture, which is quantified by the parameters Col1 fiber volume and inter-fiber distance. We previously observed in an orthotopic human breast tumor xenograft model that hypoxic tumor microenvironments reduce Col1 fiber density and increase Col1 inter-fiber distance.[19] Some of the occurring local heterogeneity in the Col1 fiber architecture of human breast cancers may be due to hypoxic pockets in these tumors. To implement SHG microscopy of Col1 fibers in the breast pathology workflow, it would be feasible to image the SHG Col1 fiber signatures using paraffin blocks generated from excised tumors of patients as was done in Fig. 3 or from biopsies as shown in Fig. 5. As SHG microscopy is nondestructive, the unaltered paraffin blocks can be returned to the pathology archive after SHG microscopic investigation. Another major advantage of SHG microscopy is that it can be performed through an ultra-compact fiber-optic endomicroscope,[40–45] which can be integrated with a 14-gauge breast biopsy needle. Such "through-needle" SHG endomicroscopy may, in the future, allow for SHG Col1 imaging to be performed during the initial diagnostic mammography-guided breast biopsy in the clinic. We have also demonstrated the feasibility of using automated software to analyze Col1 fibers and obtain robust quantitative results that avoid human subjectivity and error. Our software has the potential to provide real-time results during fiber-optic endomicroscopy scanning.

Col1 fibers are the target of recently developed stromal depletion therapies to treat desmoplasmic tumors.[46] Stromal depletion therapies are currently going into clinical trials in pancreatic cancer.[46] Imaging biomarkers that are able to assess the response to such therapies in patients will be important. The SHG-detected Col1 fiber signature may provide such a monitoring tool for stromal depletion therapies in the future, and this may be realized either by nondestructive SHG microscopy during the pathology workflow using FFPE blocks or by using SHG endomicroscopic imaging of Col1 fibers in patients. Col1 fibers also play an important role in drug delivery across the ECM of tumors, for which SHG imaging can serve as an assessment tool.[18] Tumor delivery of nanotherapeutics may in fact be improved by strategies aimed at reducing the Col1 fiber matrix, as recently demonstrated with a Col1 synthesis inhibitor in desmoplasmic models of human breast, pancreatic, and skin tumors using SHG microscopy.[47]

5 Conclusions

In summary, the results obtained here have identified a potential biomarker that may be useful in the assessment and staging of breast cancer and confirmed the importance of Col1 fibers in the metastatic process. Larger scale studies using breast and other cancer tissues are necessary to validate the sensitivity and specificity of Col1 fibers detected with SHG microscopy to predict the presence of cancer cells in lymph nodes. Such studies can lead to the development of an imaging biomarker to evaluate lymph node metastasis at the time of presentation and may result in the formulation of novel Col1 fiber-depletion strategies to reduce metastatic spread. Detection and quantification of Col1 fibers can easily be implemented in clinical pathological laboratory routines to provide additional valuable information for potentially predicting lymph node involvement in breast cancer. Automated software can be used to quantify the Col1 fiber distribution to give objective results, with the potential to perform real-time quantification during endomicroscopy.

Acknowledgments

The authors thank Dr. Scot Kuo for expert technical support with the microscopy studies on the Zeiss 710 NLO Meta confocal microscope equipped for multiphoton microscopy,

Dr. Xingde Li and Dr. Antonio Wolff for helpful discussions throughout this project, and Tiffany R. Greenwood for laboratory support. This work was supported by National Institutes of Health grants P50 CA103175 and P30 CA006973.

Authors' contributions: S. M. K. carried out all SHG imaging experiments, wrote the code of our in-house fiber analysis software, and performed all analyses with this in-house software. M. S. conceived of the in-house fiber analysis software and supervised its testing. S. S., L. K. J., P. A., and D. L. participated in the conception, design, and coordination of the study. ZMB and KG conceived of, designed, and coordinated the study. K. G. drafted the manuscript. All authors read, edited, and approved the final manuscript.

References

1. A. Bergamaschi et al., "Extracellular matrix signature identifies breast cancer subgroups with different clinical outcome," *J. Pathol.* **214**(3), 357–367 (2008).
2. M. Sund and R. Kalluri, "Tumor stroma derived biomarkers in cancer," *Cancer Metastasis Rev.* **28**(1–2), 177–183 (2009).
3. G. Falzon, S. Pearson, and R. Murison, "Analysis of collagen fibre shape changes in breast cancer," *Phys. Med. Biol.* **53**(23), 6641–6652 (2008).
4. T. Hompland et al., "Second-harmonic generation in collagen as a potential cancer diagnostic parameter," *J. Biomed. Opt.* **13**(5), 054050 (2008).
5. P. P. Provenzano et al., "Collagen reorganization at the tumor-stromal interface facilitates local invasion," *BMC Med.* **4**(1), 38 (2006).
6. P. P. Provenzano et al., "Collagen density promotes mammary tumor initiation and progression," *BMC Med.* **6**, 11 (2008).
7. M. W. Conklin et al., "Aligned collagen is a prognostic signature for survival in human breast carcinoma," *Am. J. Pathol.* **178**(3), 1221–1232 (2011).
8. G. P. Gupta and J. Massague, "Cancer metastasis: building a framework," *Cell* **127**(4), 679–695 (2006).
9. A. Lochter and M. J. Bissell, "Involvement of extracellular matrix constituents in breast cancer," *Semin. Cancer Biol.* **6**(3), 165–173 (1995).
10. A. P. Pathak et al., "Lymph node metastasis in breast cancer xenografts is associated with increased regions of extravascular drain, lymphatic vessel area, and invasive phenotype," *Cancer Res.* **66**(10), 5151–5158 (2006).
11. A. P. Pathak et al., "Characterizing extravascular fluid transport of macromolecules in the tumor interstitium by magnetic resonance imaging," *Cancer Res.* **65**(4), 1425–1432 (2005).
12. G. Alexandrakis et al., "Two-photon fluorescence correlation microscopy reveals the two-phase nature of transport in tumors," *Nat. Med.* **10**(2), 203–207 (2004).
13. D. E. Ingber, "Can cancer be reversed by engineering the tumor microenvironment?," *Semin. Cancer Biol.* **18**(5), 356–364 (2008).
14. S. Alowami et al., "Mammographic density is related to stroma and stromal proteoglycan expression," *Breast Cancer Res.* **5**(5), R129–R135 (2003).
15. T. Li et al., "The association of measured breast tissue characteristics with mammographic density and other risk factors for breast cancer," *Cancer Epidemiol. Biomarkers. Prev.* **14**(2), 343–349 (2005).
16. N. F. Boyd et al., "Heritability of mammographic density, a risk factor for breast cancer," *N. Engl. J. Med.* **347**(12), 886–894 (2002).
17. V. A. McCormack and I. dos Santos Silva, "Breast density and parenchymal patterns as markers of breast cancer risk: a meta-analysis," *Cancer Epidemiol. Biomarkers. Prev.* **15**(6), 1159–1169 (2006).
18. E. Brown et al., "Dynamic imaging of collagen and its modulation in tumors *in vivo* using second-harmonic generation," *Nat. Med.* **9**(6), 796–800 (2003).
19. S. M. Kakkad et al., "Hypoxic tumor microenvironments reduce collagen I fiber density," *Neoplasia* **12**(8), 608–617 (2010).
20. C. Bayan et al., "Fully automated, quantitative, noninvasive assessment of collagen fiber content and organization in thick collagen gels," *J. Appl. Phys.* **105**(10), 102042–102011 (2009).
21. R. Cicchi et al., "Scoring of collagen organization in healthy and diseased human dermis by multiphoton microscopy," *J. Biophoton.* **3**(1–2), 34–43 (2010).
22. W. Hu et al., "Characterization of collagen fibers by means of texture analysis of second harmonic generation images using orientation-dependent gray level co-occurrence matrix method," *J. Biomed. Opt.* **17**(2), 026007 (2012).
23. N. A. Desbiens, "A novel use for the word 'trend' in the clinical trial literature," *Am. J. Med. Sci.* **326**(2), 61–65 (2003).
24. R. M. Haralick, K. Shanmugam, and I. H. Dinstein, "Textural features for image classification," *IEEE Trans. Syst. Man Cybernet.* **SMC-3**(6), 610–621 (1973).
25. R. M. Haralick and L. G. Shapiro, *Computer and Robot Vision*, Addison-Wesley, Boston, MA (1992).
26. S. E. Singletary et al., "Revision of the American Joint Committee on Cancer staging system for breast cancer," *J. Clin. Oncol.* **20**(17), 3628–3636 (2002).
27. A. Lucci et al., "Surgical complications associated with sentinel lymph node dissection (SLND) plus axillary lymph node dissection compared with SLND alone in the American College of Surgeons Oncology Group Trial Z0011," *J. Clin. Oncol.* **25**(24), 3657–3663 (2007).
28. K. Wolf and P. Friedl, "Mapping proteolytic cancer cell-extracellular matrix interfaces," *Clin. Exp. Metastasis* **26**(4), 289–298 (2009).
29. C. T. Mierke et al., "Integrin alpha5beta1 facilitates cancer cell invasion through enhanced contractile forces," *J. Cell. Sci.* **124**(Pt 3), 369–383 (2011).
30. H. Bando et al., "The association between vascular endothelial growth factor-C, its corresponding receptor, VEGFR-3, and prognosis in primary breast cancer: a study with 193 cases," *Oncol. Rep.* **15**(3), 653–659 (2006).
31. S. Hirakawa et al., "VEGF-A induces tumor and sentinel lymph node lymphangiogenesis and promotes lymphatic metastasis," *J. Exp. Med.* **201**(7), 1089–1099 (2005).
32. K. Jennbacken et al., "Expression of vascular endothelial growth factor C (VEGF-C) and VEGF receptor-3 in human prostate cancer is associated with regional lymph node metastasis," *Prostate* **65**(2), 110–116 (2005).
33. K. Alitalo, T. Tammela, and T. V. Petrova, "Lymphangiogenesis in development and human disease," *Nature* **438**(7070), 946–953 (2005).
34. A. Grimaldi et al., "Functional arrangement of rat diaphragmatic initial lymphatic network," *Am. J. Physiol. Heart Circ. Physiol.* **291**(2), H876–H885 (2006).
35. T. J. Ryan, "Structure and function of lymphatics," *J. Invest. Dermatol.* **93**(Suppl 2), 18S–24S (1989).
36. M. A. Swartz, "The physiology of the lymphatic system," *Adv. Drug Deliv. Rev.* **50**(1–2), 3–20 (2001).
37. P. J. Campagnola and L. M. Loew, "Second-harmonic imaging microscopy for visualizing biomolecular arrays in cells, tissues and organisms," *Nat. Biotechnol.* **21**(11), 1356–1360 (2003).
38. W. R. Zipfel et al., "Live tissue intrinsic emission microscopy using multiphoton-excited native fluorescence and second harmonic generation," *Proc. Natl. Acad. Sci. U. S. A.* **100**(12), 7075–7080 (2003).
39. L. R. Cavalli, "Molecular markers of breast axillary lymph node metastasis," *Expert Rev. Mol. Diagn.* **9**(5), 441–454 (2009).
40. H. Bao et al., "Second harmonic generation imaging via nonlinear endomicroscopy," *Opt. Express* **18**(2), 1255–1260 (2010).
41. G. Liu et al., "Rotational multiphoton endoscopy with a 1 microm fiber laser system," *Opt. Lett.* **34**(15), 2249–2251 (2009).
42. M. T. Myaing, D. J. MacDonald, and X. D. Li, "Fiber-optic scanning two-photon fluorescence endoscope," *Opt. Lett.* **31**(8), 1076–1078 (2006).
43. Y. C. Wu and X. D. Li, "Two-photon fluorescence endomicroscopy," in *Advances in Lasers and Electro Optics*, N. Costa and A. Cartaxo, Eds., InTech Publishing, New York, NY (2010).
44. Y. C. Wu et al., "Scanning all-fiber-optic endomicroscopy system for 3D nonlinear optical imaging of biological tissues," *Opt. Express* **17**(10), 7907–7915 (2009).
45. Y. Wu et al., "Scanning fiber-optic nonlinear endomicroscopy with miniature aspherical compound lens and multimode fiber collector," *Opt. Lett.* **34**(7), 953–955 (2009).
46. K. Garber, "Stromal depletion goes on trial in pancreatic cancer," *J. Natl. Cancer Inst.* **102**(7), 448–450 (2010).
47. B. Diop-Frimpong et al., "Losartan inhibits collagen I synthesis and improves the distribution and efficacy of nanotherapeutics in tumors," *Proc. Natl. Acad. Sci. U. S. A.* **108**(7), 2909–2914 (2011).